ELSEVIER

Chemical Physics 253 (2000) 313–322

Chemical Physics

www.elsevier.nl/locate/chemphys

Comparative absorption, electroabsorption and electrochemical studies of intervalence electron transfer and electronic coupling in cyanide-bridged bimetallic systems: ancillary ligand effects

Fredrick W. Vance, Robert V. Slone, Charlotte L. Stern, Joseph T. Hupp *

Department of Chemistry and Materials Research Center, Northwestern University, 2145 Sheridan Road, Evanston, IL 60208, USA

Received 20 May 1999

Abstract

Electroabsorption or Stark spectroscopy has been used to evaluate the systems $(NC)_5M^{II}$–CN–$Ru^{III}(NH_3)_5^{1-}$ and $(NC)_5M^{II}$–CN–$Ru^{III}(NH_3)_4py^{1-}$, where $M^{II} = Fe^{II}$ or Ru^{II}. When a pyridine ligand is present in the axial position on the Ru^{III} acceptor, the effective optical electron transfer distance – as measured by the change in dipole moment, $|\Delta\mu|$ – is increased by more than 35% relative to the ammine substituted counterpart. Comparison of the charge transfer distances to the crystal structure of $Na[(CN)_5Fe$–CN–$Ru(NH_3)_4py] \cdot 6H_2O$ reveals that the Stark derived distances are ~50% to ~90% of the geometric separation of the metal centers. The differences result in an upward revision in the Hush delocalization parameter, c_b^2, and of the electronic coupling matrix element, H_{ab}, relative to those parameters obtained exclusively from electronic absorption measurements. The revised parameters are compared to those, which are obtained via electrochemical techniques and found to be in only fair agreement. We conclude that the absorption/electroabsorption analysis likely yields a more reliable set of mixing and coupling parameters. © 2000 Elsevier Science B.V. All rights reserved.

1. Introduction and background

Bimetallic mixed-valence complexes represent exceptionally well-defined systems for experimental interrogation of the energetics, kinetics, and dynamics of light-initiated electron transfer reactions. The amount of electron localization or delocalization present between two sites is crucial in understanding to what extent charge transfer can occur. In one extreme, where there is complete localization, the coupling between two sites will vanish, resulting in no electron transfer. In the other extreme, where complete valence delocalization has occurred, electron transfer will again cease to occur, now because the sites are too strongly coupled and the putative donor and acceptor orbitals have lost their separate identities. Thus, for electron transfer to occur, as it does in the cyanide bridged bimetallic systems described below, both the amount of coupling and the extent of valence delocalization must exist at some intermediate level. The primary goals of the current study were to critically assess and comparatively evaluate spectroscopic and electrochemical

* Corresponding author. Tel.: +1-847-491-3504; fax: +1-847-491-7713.

E-mail address: jthupp@chem.nwu.edu (J.T. Hupp).

0301-0104/00/$ - see front matter © 2000 Elsevier Science B.V. All rights reserved.
PII: S0301-0104(99)00400-0

methods for quantifying electronic coupling and residual valence delocalization. A secondary goal was to ascertain how these and related quantities, such as optical electron transfer distance, responded to subtle changes in chemical composition.

One way to describe the coupling in a bridged binuclear metal system is by applying first-order perturbation theory to a standard two-state electronic model. In this approach, based on the classic work of Mulliken and Person [1] and Hush [2], the initial and final states for charge transfer (Ψ_1 and Ψ_2) are described by linear combinations of the zeroth-order (fully localized) states, ψ_a and ψ_b:

$$\Psi_1 = c_a\psi_a + c_b\psi_b, \tag{1}$$

$$\Psi_2 = c_a^*\psi_b - c_b^*\psi_a. \tag{2}$$

The coefficients $c_a(c_a^*)$ and $c_b(c_b^*)$ can be normalized by application of Eq. (3), where S_{ab} characterizes *direct* overlap between the orbitals a and b:

$$c_a^2 + c_b^2 \pm 2c_ac_bS_{ab} = 1. \tag{3}$$

If the overlap is small enough to be neglected ($S_{ab} \ll 1$), and a two-state analysis is appropriate, then the ground and excited state coefficients should be identical, i.e., $c_a^* = c_a$ and $c_b^* = c_b$. Under this condition, the squares of the coefficients themselves describe the fractional amount of charge present at each site; a c_b^2 value of zero indicates complete valence localization, whereas a c_b^2 value of 0.5 indicates complete *de*localization. Although this type of description was first utilized in only weakly coupled systems (i.e., in the perturbation limit), more recent work has indicated that it can also be applied to strongly coupled systems (provided that the two-state description remains applicable) [3,4].

In order to understand the dynamics of charge transfer, it is useful to quantitate the electronic coupling matrix element, H_{ab} on which the rate of electron transfer (in the nonadiabatic limit) strongly depends. This can be accomplished by solving the secular determinant for Eqs. (1) and (2), leading to Eq. (4) [3]:

$$H_{ab} = \frac{\mu_{12}E_{op}}{eR_{ab}}. \tag{4}$$

In Eq. (4), μ_{12} is the transition moment, E_{op} is the energy of the optical transition, e is the unit electron charge, and R_{ab} is the diabatic charge transfer distance (effective one-electron transfer distance). The key point is that an accurate estimation of the electronic coupling parameter via Eq. (4) requires a knowledge of the effective charge transfer distance, which can be directly ascertained via electroabsorption (Stark) spectroscopy (vide infra).

Recent studies have shown that for $(CN)_5Fe^{II}$–CN–$Ru^{III}(NH_3)_5^-$ (**1**) and $(CN)_5Ru^{II}$–CN–$Ru^{III}(NH_3)_5^-$ (**3**), the effective charge transfer distance is only about one half the geometric separation of the donor and acceptor [5]. [1] Previous work has shown that substitution at the axial position on the acceptor has interesting effects on both the electrochemistry and linear optical properties of a related chromophore [6]. The goals of this work are to evaluate $\Delta\mu_{12}$, R_{ab}, and by inference, electronic coupling, via electroabsorption spectroscopy and to compare the parameters to those obtained electrochemically for compounds **1** and **3** as well as their pyridine containing derivatives.

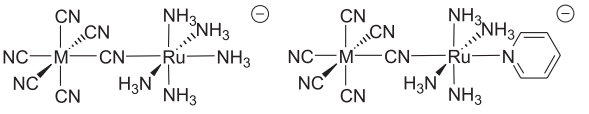

1 M=Fe, **3** M=Ru **2** M=Fe, **4** M=Ru

[1] For a related report, see Ref. [17] in which the authors report $\Delta\mu_{12}\mathbf{F}_{int}/\mathbf{F}_{external}$ values, rather than $\Delta\mu_{12}$ values, where the numerical difference in the two types of parameters is estimated here to be on the order of 30%. Note also that the parameters in their report would be classified as "adiabatic" parameters in the analysis used here.

2. Experimental section

2.1. Syntheses

Compounds **1**–**4** were prepared by the literature methods [6–8], which produce sodium salts with varying degrees of Na_2SO_4 contamination [6]. In order to minimize such contaminations, the compounds were purified by recrystallization from H_2O/MeOH (1:2) and passed through a size exclusion (Bio-Gel P-2) column. In order to grow crystallographic quality crystals, a sample of **2** was dissolved in minimal H_2O. A twofold excess of methanol was then layered on top, and the two-phase system was allowed to stand at ~5°C for ~24 h. The dark green crystals were removed from the solution via filtration and washed with a very small amount of H_2O to remove the residual pale green powder. X-ray crystallography: primitive monoclinic cell, space group = $P2_1/n$ (No. 14), $a = 9.8081$ Å, $b = 15.3965$ Å, $c = 15.3018$ Å, $\beta = 90.1510°$, $V = 2310.7346$ Å^3, $Z = 4$, $R = 0.045$ and goodness of fit = 1.95 (see supporting information for more details). The solid was determined to be $Na[(CN)_5–Fe–CN–Ru(NH_3)_4–py]\cdot 6H_2O$ (FW = 591.33), and was free of electroactive impurities via cyclic voltammetry (CV).

2.2. Electrochemistry

CV was performed on all the samples to screen for electroactive impurities and to evaluate the formal potentials of the metal centers. A 0.01 cm^2 glassy carbon electrode was used as the working electrode, with a platinum counter electrode and a saturated calomel reference electrode. Scan rates typically ranged from 20 to 100 mV/s. All samples were dissolved in water with 0.1 M KCl present as an electrolyte.

Rotating disk electrochemistry (RDE) was also performed in order to evaluate the concentrations of solutions. A 0.25 cm^2 glassy carbon electrode was used as the working electrode, with the other electrodes being the same as for the CV experiment. Rotation rates were varied between 800 and 1600 rpm, with voltage scan rates ranging from 5 to 20 mV/s. The results were evaluated by measuring the amount of current passed through a known concentration of compound **3** (measured by absorption using the published extinction coefficient [9]), and comparing this to the current passed through solutions of unknown concentration. By this method, the concentrations of compounds **2** and **4** could be quantitatively evaluated for subsequent spectral analyses.

2.3. Electronic absorption

Absorption spectra were recorded on an OLIS modified Cary-14 spectrophotometer. A 0.1 cm quartz cell was used to quantitate absorption in the region from 360 to 2100 nm, covering the entire charge transfer region. Chromophores were examined in the same solutions (0.1 M KCl in water) as for the RDE experiment to determine extinction coefficients. In order to obtain reliable line shapes in the extended near infrared wavelength region, D_2O was used as a solvent in place of H_2O.

2.4. Electroabsorption

The Stark effect spectroscopy was done in a manner described fully elsewhere, [10–12] by using a PMT for visible detection and both InGaAs and Si photodiode detectors for studies in the near infrared (NIR) region. (For compound **2**, data obtained with InGaAs and Si photodiodes were pieced together in order to facilitate fitting over the entire spectral range). Compounds were studied in a solvent glass of ethylene glycol and H_2O in the ratio 1:1 (v:v) for experiments in the visible region and in a glass of ethylene glycol and D_2O in the ratio 1:1 for experiments in the NIR region.

3. Results

3.1. X-ray crystallography

Fig. 1 shows an ORTEP drawing of compound **2**. Several features are noteworthy. The most striking, perhaps, is that the C–N–Ru bond is bent at an angle of 164°, as opposed to the linear structure expected. This is most likely due to

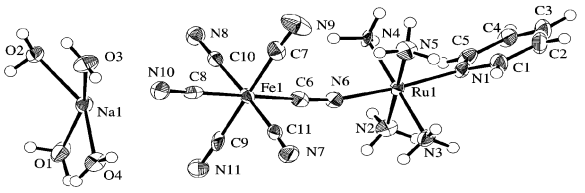

Fig. 1. ORTEP rendering of compound **2** shows the bent nature of the Fe^{II}–CN–Ru^{III} bonds. Also notice the coordinated sodium cation with four solvating H_2O molecules on the left. Two of the H_2O molecules (not shown) were found to be slightly disordered, and thus the hydrogens were not explicitly solved for.

packing forces in the crystal, as other structural features indicate. The first is that the pyridine ligand is contorted as well. The angle between the Ru–py bond and the plane of the pyridine is bent to a similar angle of 168°. Additional evidence can be found from analysis of the equatorial ammonia ligands, where a variation in the Ru–N bond length is seen. The two ligands on the same plane as the C–N–Ru bend are found to be compressed by roughly 0.02 Å relative to those perpendicular to the bend. Thus the metal–metal separation distance in solution is probably best estimated by addition of the (crystallographically determined) lengths of the bonds between them (5.05 Å), rather than by the minimum distance between the metal centers in the crystal structure (4.9 Å).

The other intriguing result from the crystal structure is the rather high degree to which the octahedra of the two metal centers are aligned. Despite the bent nature of the structure, the improper dihedral angle between the equatorial cyanide and corresponding equatorial ammine ligands is less than 12°.

3.2. Electrochemistry

The electrochemical study of compounds **3** and **4** revealed a metal-localized *trans* ligand redox sensitivity essentially identical to that previously reported for compounds **1** and **2** [6]. As shown in Fig. 2, substitution on the Ru^{III} center perturbed not only the formal potential of that site, but also of the adjacent donor Ru^{II} center. The measured formal potentials (mV vs. SSCE) were as follows:

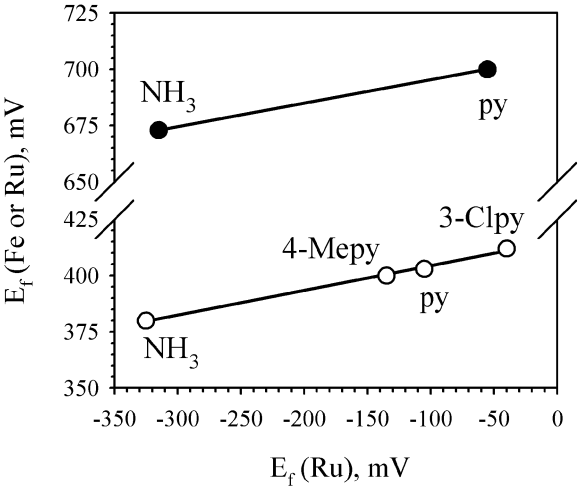

Fig. 2. Donor metal (Fe^{II} or Ru^{II}) formal potential versus acceptor metal (Ru^{III}) formal potential shows perturbations of both sites due to substitutions on the acceptor. (● = Ru^{II} donor, slope = 0.10; ○ = Fe^{II} donor, slope = 0.11, additional data from Ref. [6].)

(1) E(Fe) = 380, E(Ru) = −325; (2) E(Fe) = 403, E(Ru) = −105; (3) E(Ru) = 673, E(Ru) = −315; (4) E(Ru) = 700, E(Ru) = −55.

Curtis and coworkers have shown [13,14] that when a perturbation is applied at the acceptor site, the amount of delocalization for a system may be related to the changes in the formal potentials of the donor (δE_1) and acceptor (δE_2) by Eq. (5) [13]:

$$\frac{\delta E_1}{\delta E_2} = \frac{c_b^2}{c_a^2}, \tag{5}$$

where c_a and c_b are the mixing coefficients described in Eqs. (1)–(3), and S_{ab} is assumed to be zero. Returning to Fig. 2, the unitless slopes are 0.11 and 0.10 for the Fe^{II}–Ru^{III}–Y^- series and the Ru^{II}–Ru^{III}–Y^- pair, respectively. Eq. (5) then yields respective values for c_b^2 of 0.10 and 0.09. In conjunction with the absorption data, the delocalization parameter can be used to determine H_{ab} through Eq. (6) [4]:

$$H_{ab}^2 = (c_b^2 - c_b^4)E_{op}^2. \tag{6}$$

This relation again utilizes Eq. (3) under the conditions, where the overlap is small ($S_{ab} \ll 1$). Implementation of Eq. (6) yields values between 2500

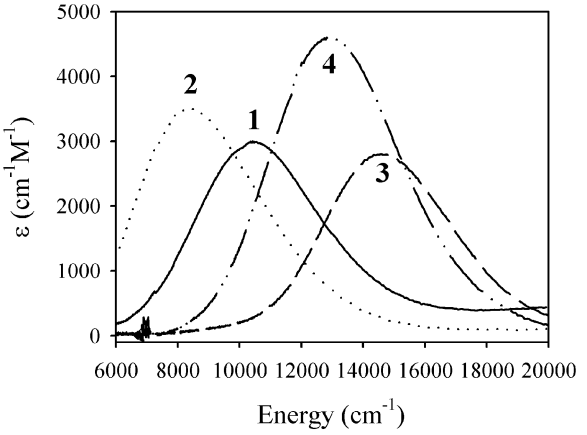

Fig. 3. Absorption spectra for compounds **1**–**4** show that pyridine substituted derivatives (**2** and **4**) have charge transfer bands that are lower in energy and have higher extinction coefficients (ε).

and 4200 cm^{-1} for H_{ab} for compounds **1**–**4** (see Table 2).

3.3. Absorption

The primary effect of substitution of an axial NH_3 for pyridine is a lowering of the energy of the optical charge transfer transition. As shown in Fig. 3, however, modest differences in the molar extinction coefficients can also be introduced. Intervalence bandwidths, on the other hand, are essentially unaffected (see Table 1).

3.4. Electroabsorption

Electroabsorption (Stark) spectroscopy readily provides two quantities associated with an electronic transition: (1) the absolute change in dipole moment upon excitation, $|\Delta\mu_{12}|$, and (2) the trace of the change in polarizability, $\mathrm{Tr}(\Delta\alpha_{12})$. The quantities are obtained via a simplified version of Liptay's analysis [15], which compares the Stark spectrum, $\Delta A(\bar{\nu})$, to derivatives of the absorption spectrum, $A(\bar{\nu})$:

$$\Delta A(\bar{\nu}) = \left\{ A_\chi A(\bar{\nu}) + \frac{B_\chi \bar{\nu}}{15hc} \frac{\mathrm{d}[A(\bar{\nu})/\bar{\nu}]}{\mathrm{d}\bar{\nu}} + \frac{C_\chi \bar{\nu}}{30h^2c^2} \frac{\mathrm{d}^2[A(\bar{\nu})/\bar{\nu}]}{\mathrm{d}\bar{\nu}^2} \right\} \mathbf{F}_{\mathrm{int}}^2. \quad (7)$$

In Eq. (7), $\bar{\nu}$ is the wave number of the absorbed light (cm^{-1}), h is Planck's constant, c is the speed of light, and $\mathbf{F}_{\mathrm{int}}$ is the internal electric field. $\mathbf{F}_{\mathrm{ext}}$ is related to the externally applied field, by $\mathbf{F}_{\mathrm{int}} = f\mathbf{F}_{\mathrm{ext}}$, where f is a function of the static dielectric constant, D_s. If the molecule is considered to reside in a spherical cavity in a medium with a static dielectric constant of D_s, the local field correction factor is $f = 3D_s/(2D_s + 1)$. Low temperature capacitance measurements have previously been used to derive an f value of 1.3 using a spherical cavity for the solvent system used in this study [11]. (It should be noted that a recent work [16] has suggested that continuum models such as this may underestimate f as freezing may increase the local polarity around a molecule.) The resulting coefficients A_χ, B_χ, and C_χ have been described in detail previously [17]. Briefly, however, they provide information, respectively, about changes in the transition moment, the polarizability, and the permanent dipole moment. As shown in Fig. 4 for compound **2**, the electroabsorption spectra of these complexes is dominated by changes in the dipole moment (coefficient C_χ from Eq. (7)),

Table 1
Summary of electroabsorption and absorption results

Compound	$\lvert\Delta\mu_{12}\rvert$ (eÅ)	$\mathrm{Tr}(\Delta\alpha_{12})$ (Å^3)	E_{op}[a] (cm^{-1})	$\Delta\nu_{1/2}$[a] (cm^{-1})	ε_{max}[a] (cm^{-1})
1. $(CN)_5Fe^{II}$–CN–$Ru^{III}(NH_3)_5^{1-}$	2.4[b]	230[b]	10,300	4840	3000[c]
2. $(CN)_5Fe^{II}$–CN–$Ru^{III}(NH_3)_4py^{1-}$	4.5	1100	8,300	4560	3500
3. $(CN)_5Ru^{II}$–CN–$Ru^{III}(NH_3)_5^{1-}$	2.8[b]	450[b]	14,600	4900	2800[c]
4. $(CN)_5Ru^{II}$–CN–$Ru^{III}(NH_3)_4py^{1-}$	3.8	460	12,800	4970	4600

[a] From room temperature absorption in water as a solvent.
[b] From Ref. [5].
[c] From Ref. [9].

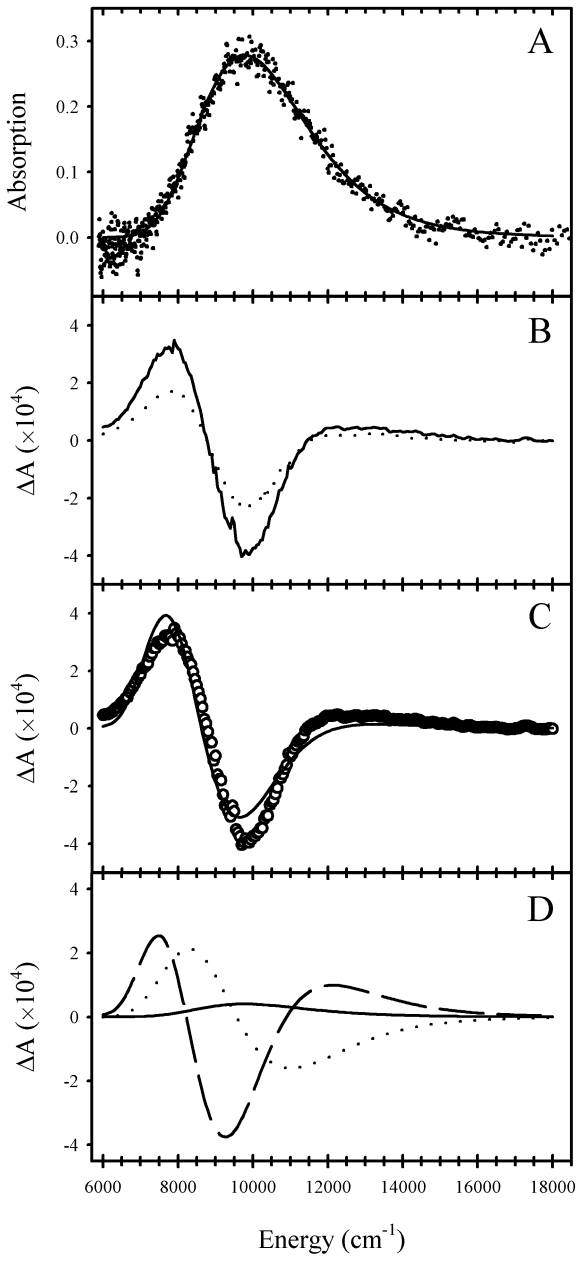

Fig. 4. (A) Absorption spectrum for **2** (·) recorded at 77 K with a fit to the Gaussian curve (—). (B) Electroabsorption spectra at angles of 55° (—) and 90° (– – –). (C) Least-squares fit (—) of 55° data (○) to Eq. (6). (D) Zeroth (—), first (· · ·) and second (– – –) derivative contributions to the 55° fit from panel C.

corroborating the charge transfer nature of these transitions.

Perhaps, the most interesting finding of this study is that replacement of nominally innocent ancillary ligands in bridged bimetallic system can exert significant effects upon the change in dipole moment, $\Delta\mu_{12}$, accompanying metal-to-metal charge transfer. Replacing an ammonia molecule with pyridine in the *trans* position of the acceptor metal ion substantially increases the effective adiabatic charge transfer distance, R_{12}:

$$\Delta\mu_{12} = eR_{12}. \tag{8}$$

In Eq. (8), e is the electron unit charge (see Table 1). Although the existence of the ligand substitution effect is, in retrospect, readily rationalized based on standard inorganic chemical bonding considerations, it should be noted that R_{12} has usually been equated simply with the physical distance between the nominal donor and acceptor atoms [4, 18 and references therein], the physical or geometric separation, of course, is barely altered by ancillary ligand replacement. To the best of our knowledge, the experiments involving **1**–**4** are the first to demonstrate explicitly that the ancillary environment exerts a significant effect upon the effective one-electron transfer distance.

Less clear is the effect of ancillary ligand substitution upon the change in polarizability, $\mathrm{Tr}(\Delta\alpha_{12})$. The Liptay analysis indicates that in each case an easily observable component of the experimental Stark signal can be attributed to a first derivative component. (For simplicity, we have assumed that this component is entirely due to the $\mathrm{Tr}(\Delta\alpha_{12})$ term, neglecting possible contributions from product terms of α and $\Delta\mu$ [5].) Nevertheless, given the quality of the spectral fits, we are reluctant to attach particular significance to the *differences* in $\mathrm{Tr}(\Delta\alpha_{12})$ values among the compounds.

4. Discussion

4.1. Ligand effects

The longer charge transfer distances for compounds **2** and **4** (relative to **1** and **3**, respectively)

can be rationalized by considering the effect of adding a π-acceptor to the Ru^{III} center. Although Ru^{III} is a relatively poor π donor, Ru^{II} is considerably more effective. It follows that formation of Ru^{II} in the excited state (from Ru^{III} in the ground state) will enhance the metal center's ability to donate electron density to the pyridine ligand. In a one-electron picture, the effect of the electron donation to the *trans* pyridine ligand would be to place the transferred charge in the electronic excited state somewhat further from the ground-state electron donor ($M^{II}(CN)_6$ fragment) than would be the case if the ligand were not capable of behaving as a π acceptor. According to this argument: (a) addition of electron withdrawing groups such as Cl, F, or NO_2 to the *trans* pyridine ligand should further extend the effective one-electron transfer distance, but (b) similar ligand alterations *cis* to the bridge (i.e. orthogonal to the bridge) should have little effect upon the effective one-electron transfer distance.

The electroabsorption experiments also provide information about changes in molecular polarizability. We [5] and others [19,20] have previously noted that both the positive signals and comparatively large magnitudes of $Tr(\Delta\alpha_{12})$ are indicative of multiple upper excited state participation in the nominally intervalence charge transfer transitions. Indeed, the polarizability parameter appears to be much more clearly diagnostic of such participation than does the distance or dipole-moment-difference parameter.

4.2. Degeneracy

The crystal structure of compound **2** provides an important insight into the nature of IVCT transitions for this family of compounds. This transition can, in principle, involve either degenerate orbital on the iron or ruthenium donor (d_{xz} or d_{yz}; z is the long axis of the molecule), suggesting that the transition is doubly degenerate. However, since the octahedra of the two metal centers are well aligned for **2** (and presumably **1**, **3**, and **4**), it is likely that only one of these will effectively overlap with the single available acceptor orbital (either d_{xz} or d_{yz}) on the ruthenium center. Thus, since donation only occurs to one orbital, the appropriate degeneracy is one.

For compounds **2** and **4**, the degeneracy of the d_{xz} and d_{yz} acceptor orbitals is removed by the presence of the pyridine ligand. Since the plane of the ring is at roughly 37° with respect to the ammonia–ruthenium–ammonia plane, the π overlap will be greater for one d orbital than the other, effectively splitting the orbitals energetically.

4.3. Electronic coupling

The electrochemical studies of compounds **1**–**4** have been used to conclude that the extent of delocalization as measured by c_b^2 is a factor of 3–5 greater than that derived solely from oscillator strength measurements [9] (assuming a "geometric" metal–metal charge transfer distance, see Table 2). It is possible that the discrepancy is due to the fact that the charge transfer distance (from Eq. (4), Table 1) within these chromophores is significantly smaller than the geometric separation of the donor and acceptor of 5.05 Å, derived from crystallographic measurements.

To evaluate this suggestion, the results from Stark spectroscopy can be used to assess the mixing parameter c_b^2. Toward this end, we must first

Table 2
Electronic coupling and delocalization parameters

Compound	H_{ab}[a] (cm^{-1})	H_{ab}[b] (cm^{-1})	H_{ab}[c] (cm^{-1})	c_b^{2a}	c_b^{2b}	c_b^{2c}
1	1600	2800	3100	0.024	0.080	0.10
2	1500	1600	2500	0.033	0.036	0.10
3	1800	3000	4200	0.016	0.044	0.09
4	2200	2700	3700	0.031	0.045	0.09

[a] From absorption experiments utilizing geometric separation of donor and acceptor (5.05 Å).
[b] From absorption and electroabsorption (Stark) experiments.
[c] From electrochemical experiments. Note that this method produces only one c_b^2 value for each family of compounds.

extrapolate the distance parameters results to the diabatic limit (designated by *ab* subscripts), as outlined in Eqs. (9) [4] and (10) [3]:

$$\mu_{12} = 2.07 \times 10^{-2} \left(\frac{\varepsilon_{\max} \Delta \nu_{1/2}}{E_{\mathrm{op}}} \right)^{1/2}, \tag{9}$$

$$\Delta\mu_{ab} = eR_{ab} = (\Delta\mu_{12}^2 + 4\mu_{12}^2)^{1/2}. \tag{10}$$

Here μ_{12} is the transition moment (eÅ), $\varepsilon_{\max}$ is the molar extinction coefficient at the band maximum (cm^{-1} M^{-1}), $\Delta\nu_{1/2}$ is the bandwidth determined by the full width at half maximum (cm^{-1}), and E_{op} is the absorption maximum (cm^{-1}). A comparison to the electrochemical experiments is then accomplished by evaluating the mixing parameter, c_b^2, via Eq. (11):

$$c_b^2 = \frac{1}{2}\left[1 - \left(\frac{\Delta\mu_{12}^2}{\Delta\mu_{12}^2 + 4\mu_{12}^2}\right)^{1/2}\right] = \frac{1}{2}\left(1 - \frac{\Delta\mu_{12}}{\Delta\mu_{ab}}\right). \tag{11}$$

Although the new results (Table 2) indicate a higher degree of delocalization than did the original spectroscopic studies [9], they point to a lower degree of delocalization than do the electrochemical investigations. (Recall that the electrochemical analysis is unaffected by revisions in the effective charge transfer distance.)

The discrepancy between the electrochemical and Stark derived estimates for c_b^2 (again see Table 2) is somewhat surprising, in view of the essentially identical levels of theoretical approximation inherent to the two analyses (first-order perturbation, two-state limit, neglect of direct orbital overlap, etc.). Watzky and co-workers have pointed out, however, that additional factors, such as substitution-induced changes in solvational free energies, can, in principle, contribute to the electrochemical response [21]. In addition, in implementing the electrochemical analysis, we assumed that metal orbital mixing effects are finite for $(NC)_5M^{II}$–CN–$M'^{III}(NH_3)_4Y^{1-}$ species but zero for the $(NC)_5M^{III}$–CN–$M'^{III}(NH_3)_4Y^{0}$ and $(NC)_5M^{II}$–CN–$M'^{II}(NH_3)_4Y^{2-}$ forms. While the distinctions regarding degrees of mixing clearly are qualitatively correct, it is conceivable that they fail to an experimentally significant extent in quantitative studies. A third point is that the electrochemical analysis necessarily assumes that the degree of orbital mixing is identical for all members of a given series of compounds – an assumption that is not supported by the Stark based optical analysis (which provides mixing or coupling information separately for each compound examined).

Finally, the electrochemical experiments interrogate orbital mixing in a ground electronic configuration by postulating coupling to a vibrationally relaxed "redox isomer", $(NC)_5M^{III}$–CN–$M'^{II}(NH_3)_4Y^{1-}$. The absorption based analysis, on the other hand, probes both ground and excited state species, where the excited state is in the Franck–Condon region, i.e., the electronic excited state ($(NC)_5M^{III}$–CN–$M'^{II}(NH_3)_4Y^{1-}$) is also vibrationally excited (see Fig. 5). In a strict two-state treatment (Mulliken–Hush treatment), the distinction is unimportant; orbital mixing (delocalization) occurs to identical extents in the

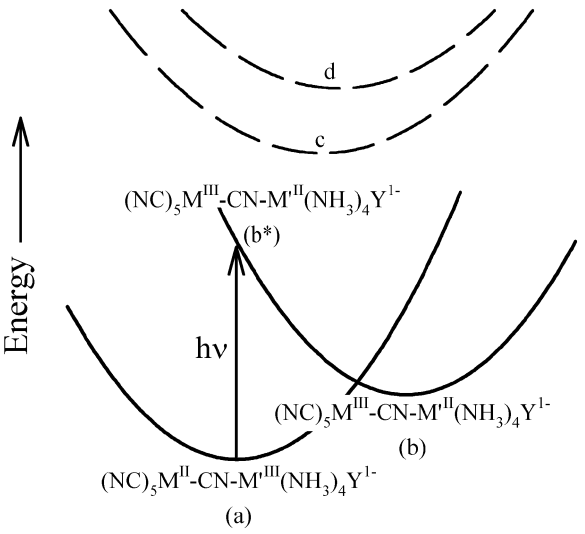

Fig. 5. Nonadiabatic ground and excited state surfaces (arbitrarily scaled). Note that the optical experiment probes coupling between states a and b*, whereas the electrochemical experiment probes the coupling between states a and b. Also note from purely energetic arguments that coupling between state b* and higher excited states (c and d) should be much stronger than coupling between either a or b and the same excited states (c or d).

ground versus excited electronic states. Furthermore, initial-state/final-state electronic coupling is independent of the degree of vibrational excitation. In real systems, however, higher lying excited states always exist and, therefore, configuration interactions must be considered. From an admittedly simplistic energy gap argument, these interactions are likely to be greater for an excited state prepared in the Franck–Condon region than for either a vibrationally relaxed electronic excited state or a ground electronic state. Indeed, this notion is supported by the Stark-derived $\mathrm{Tr}(\Delta\alpha)$ data discussed above and elsewhere [5,19].

Based on the above discussion, we suggest that the Stark-based optical analysis likely provides more reliable orbital mixing and electronic coupling information than does the electrochemical analysis. On the other hand, the electrochemical technique is in some respects quite attractive. Most notably, it altogether avoids the uncertainties accompanying the treatment of internal field corrections in the Stark analysis.

5. Conclusions

Stark spectroscopy of cyanide-bridged binuclear metal complexes shows that the effective one-electron charge transfer distance (metal-to-metal charge transfer) can be changed by changing the chemical identity of an ancillary ligand. The experiments additionally indicate, consistent with earlier measurements, that the effective charge transfer distance can be significantly shorter than the crystallographically defined metal–metal separation distance. Use of the shorter distance in a Mulliken–Hush analysis of electronic delocalization parameters (c_b^2) and initial-state/final-state electronic coupling parameters (H_{ab}) yields parameters that are significantly larger than those obtained by using the crystallographic distance. A comparison of the parameters to those obtained via an alternative electrochemical analysis indicates only fair agreement, with the electrochemical analysis returning somewhat larger estimates. Based on several admittedly tangential considerations, we conclude that the absorption/electroabsorption analysis likely provides better estimates of two-state electronic coupling and orbital mixing parameters.

Acknowledgements

We acknowledge helpful discussions with Dr. Marshall Newton and Prof. Jeff Curtis. We thank the US Department of Energy, Office of Research, Division of Chemical Sciences (Grant No. DE-FG02-87ER13808). FWV thanks the Materials Research Center at Northwestern University (Grant No. NSF-DMR-9632472) for a graduate assistantship.

Supporting Information Available: A description of X-ray crystallographic information, including a CIF format file, is available.

References

[1] R.S. Mulliken, W.B. Person, Molecular Complexes, Wiley, New York, 1969.
[2] N.S. Hush, Prog. Inorg. Chem. 23 (1984) 3002.
[3] R. Cave, M.D. Newton, Chem. Phys. Lett. 249 (1996) 15.
[4] C. Creutz, M.D. Newton, N. Sutin, J. Photochem. Photobiol. A. Chem. 82 (1994) 47.
[5] F.W. Vance, L. Karki, J.K. Reigle, J.T. Hupp, M.A. Ratner, J. Phys. Chem. A102 (1998) 8320.
[6] Y. Dong, J.T. Hupp, Inorg. Chem. 31 (1992) 3170.
[7] A. Vogler, J. Kisslinger, J. Am. Chem. Soc. 104 (1982) 2311.
[8] A. von Kameke, G.M. Tom, H. Taube, Inorg. Chem. 17 (1978) 1790.
[9] A. Burewicz, A. Haim, Inorg. Chem. 27 (1988) 1611.
[10] L. Karki, H.P. Lu, J.T. Hupp, J. Phys. Chem. 100 (1996) 15637.
[11] L. Karki, J.T. Hupp, J. Am. Chem. Soc. 119 (1997) 4070.
[12] L. Karki, J.T. Hupp, Inorg. Chem. 36 (1997) 3318.
[13] R. de la Rosa, P.J. Chang, F. Salaymeh, J.C. Curtis, Inorg. Chem. 24 (1985) 4229.
[14] F. Salaymeh, S. Berhane, R. Yusof, R. de la Rosa, E.Y. Fung, R. Matamoros, K.W. Lau, Q. Zheng, E. Kober, J.C. Curtis, Inorg. Chem. 32 (1993) 3895.
[15] R. Wortmann, K. Elich, W. Liptay, Chem. Phys. 124 (1988) 395.
[16] G.U. Bublitz, S.G. Boxer, J. Am. Chem. Soc. 120 (1998) 3988.
[17] G.U. Bublitz, S.G. Boxer, Annu. Rev. Phys. Chem. 48 (1997) 213.
[18] P.F. Barbara, T.J. Meyer, M.A. Ratner, J. Phys. Chem. 100 (1996) 13148.

[19] Y.K. Shin, B.S. Brunschwig, C. Creutz, N.J. Sutin, Phys. Chem. 100 (1996) 8157.
[20] D.H. Oh, M. Sano, S.G. Boxer, J. Am. Chem. Soc. 113 (1991) 6880.
[21] M.A. Watzky, A.V. Macatangay, R.A. Van Camp, S.E. Mazzetto, X. Song, J.F. Endicott, T. Burranda, J. Phys. Chem. A101 (1997) 8441.